CRITICAL REVIEW

CSR
www.rsc.org/csr

Matrix infrared spectra and density functional calculations of transition metal hydrides and dihydrogen complexes

Lester Andrews
Department of Chemistry, University of Virginia, P. O. Box 400319, Charlottesville, VA 22904-4319; Tel: 434-924-3513; Fax: 434-924-3710. E-mail: lsa@virginia.edu

Received 12th June 2003
First published as an Advance Article on the web 30th January 2004

Metal hydrides are of considerable importance in chemical synthesis as intermediates in catalytic hydrogenation reactions. Transition metal atoms react with dihydrogen to produce metal dihydrides or dihydrogen complexes and these may be trapped in solid matrix samples for infrared spectroscopic study. The MH_2 or $M(H_2)$ molecules so formed react further to form higher MH_4, $(H_2)MH_2$, or $M(H_2)_2$, and MH_6, $(H_2)_2MH_2$, or $M(H_2)_3$ hydrides or complexes depending on the metal. In this *critical review* these transition metal and dihydrogen reaction products are surveyed for Groups 3 though 12 and the contrasting behaviour in Groups 6 and 10 is discussed. Minimum energy structures and vibrational frequencies predicted by Density Functional Theory agree with the experimental results, strongly supporting the identification of novel binary transition metal hydride species, which the matrix-isolation method is well-suited to investigate. 104 references are cited.

1 Introduction

Transition metals and their compounds catalyze reactions of H_2 with organic molecules, which is the basis of catalytic hydrogenation. Classical metal hydrides (L_nMH_2) were known to be part of the catalytic cycle, but nonclassical dihydrogen complexes ($L_nM(H_2)$) were only assumed to be intermediates until the first example was discovered and characterized by Kubas *et al.*[1] Thus, the hidden phenomenon of molecular hydrogen coordination and activation of H–H bonds was brought to light. The over 350 known stable complexes involve every metal from V to Pt. Only the very early transition metals and actinides are not represented.[2,3]

Most transition metal H_2 complexes are cationic because the higher electrophilicity of the cation site reduces the back donation that leads to oxidative addition and dihydride formation. The coordination chemistry of dihydrogen has been reviewed extensively,[2–5] and the equilibrium isotopic effects of H_2 and D_2 in the Kubas complex have demonstrated that D_2 is bound (8.6 ± 0.5 kcal mol^{-1}) slightly stronger than H_2 (6.8 ± 0.5 kcal mol^{-1}).[6] In addition, photochemical mechanisms for reductive elimination of H_2 from organometallic dihydride complexes have been described.[7] However, naked metal atoms or metal hydrides also form dihydrogen complexes, and the matrix-isolation technique is a proven method for bringing metal atoms and small molecules together, isolating them from gross solvent effects, and investigating their mutual interaction and photochemistry. This method typically relies on infrared spectroscopy and compares the effect of complexation on the vibrational spectra of the parent molecules. However, naked metal hydrides and dihydrogen complexes *without ligands* are therefore fundamentally different from organometallic hydride complexes: the naked metal species are unsaturated, and thus more reactive and they interact differently with molecular H_2.

The celebrated example of a naked metal dihydrogen complex is $Pd(H_2)$. This complex, which forms spontaneously from Pd and H_2, was first discovered by Ozin and Garcia-Prieto[8] and later reaffirmed in collaborative work from this laboratory and that of Manceron.[9] The later work also formed higher bis and tris complexes with additional dihydrogen available. Several metal monohydrides, dihydrides, and trihydrides also form dihydrogen complexes as will be discussed in this review. Some of these complexes undergo equilibration between the dihydrogen complex and dihydride subunits in the matrix as reported for the Kubas complex $W(CO)_3(PR_3)_2(\eta^2\text{-}H_2)$ at room temperature in solution[10] which, based on the low H–H stretching mode and the observed W–H stretching modes, is well along the reaction coordinate to oxidative addition.[1,6] However, the related $Cr(CO)_5(H_2)$ complex prepared by Sweany in rare gas matrices[11] and in larger yield (along with Mo and W counterparts) by Upmacis *et al.* in liquid xenon under H_2 pressure such that the H–H stretching modes could be observed[12] is stable for only a few seconds at room temperature. Finally, an investigation of the naked W atom reaction with H_2 in excess neon revealed WH_2 and WH_4, and led to the discovery of WH_6 in the trigonal prismatic classical hydride structure predicted by theory.[13–15] Unfortunately, it is not possible to determine the thermal stability of WH_6 because of reactive aggregation while the matrix evaporates.

After describing the experimental and theoretical methods used to prepare and characterize naked metal hydrides and dihydrogen complexes, several examples of dihydrides, trihydrides, tetrahydrides, and hexahydrides will be discussed. Particular attention will be paid to the mode of dihydrogen bonding and to vertical relationships in the periodic table.

Lester Andrews has been a chemistry professor at the University of Virginia since 1966 after earning a PhD with Professor George Pimentel at the University of California, Berkeley. He has specialized in matrix infrared spectroscopy of novel molecules such as molecular ions, complexes, metal hydrides, and transient species. This work combines cryogenic technology with chemical and physical methods for generating new molecular species. Lester Andrews has authored or co-authored over 600 research publications. He has enjoyed Fulbright Senior Research Fellowships at Southampton and Oxford Universities. His current research interests involve laser-ablation to produce metal atoms for reaction with small molecules during condensation in excess argon, neon, and hydrogen.

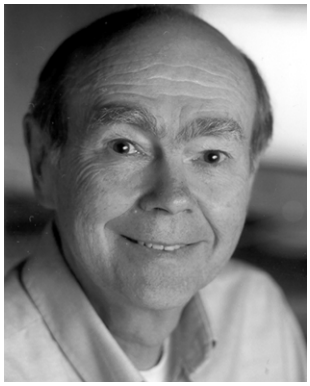

DOI: 10.1039/b210547k

2 Experimental and computational methods

The experiment for reactions of laser-ablated transition metal atoms with small molecules during condensation in excess argon and neon has been described in detail previously.[16,17] Fig. 1 illustrates the

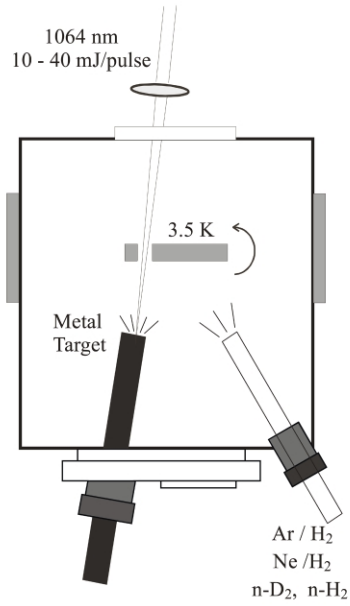

Fig. 1 Schematic diagram of apparatus for laser-ablation matrix-isolation infrared spectroscopic investigation of transient species. After matrix/reagent/metal co-deposition, the cold window is rotated 90° for recording infrared spectra, as indicated by the arrow. The infrared beam from the spectrophotometer is normal to the outside CsI optical windows.

experimental approach. The Nd:YAG laser fundamental (1064 nm, 10 Hz repetition rate with 10 ns pulse width) was focused onto a rotating metal target, and the laser energy was varied from 10–40 mJ pulse^{-1}. Thus, laser-ablated metal atoms were co-deposited with hydrogen molecules in excess argon, neon, or pure hydrogen as the matrix and reagent[18,19] onto a 3.5 K CsI cryogenic window using a Sumitomo Heavy Industries Model RDK-205D closed-cycle cryocooler. Hydrogen, D_2, HD, and $H_2 + D_2$ mixtures were used in different experiments. Fourier-transform infrared spectra were recorded at 0.5 cm^{-1} resolution on a Nicolet 750 with 0.1 cm^{-1} accuracy using an Hg–Cd–Te detector. Matrix samples were annealed at different temperatures, and selected samples were subjected to broadband photolysis by a medium-pressure mercury arc lamp (Philips, 175W) with globe removed (240–700 nm).

Thermal methods have traditionally been employed to evaporate transition metal atoms.[8,9,20–23] However, laser-ablation has some advantages over thermal evaporation as a source of metal atoms (plus a small yield of cations and electrons).[17] First, laser-ablated atoms have excess kinetic/electronic energy.[24] Second, the refractory metals like tungsten can be evaporated.[13] Third, minimum heat load is put on the matrix substrate as only a small volume of metal is heated to very high temperature. However, the major disadvantage is laser-induced emission from the target surface, which irradiates the sample, but this can be used to advantage! Hydrogen is the most difficult molecule to trap in a matrix. Hence, the substrate must be as cold as possible, no more than 10 K for argon and 4 K for neon, and 4 K or less for pure hydrogen and deuterium. The earlier Pd(H_2) work employed krypton and xenon matrices because the cryogenic refrigerator could not get cold enough to trap H_2 in solid argon.[8,9]

These matrix hosts are different and each presents some advantages and disadvantages. For a common substrate temperature, such as 3.5 K currently employed in our laboratory, argon freezes more rapidly and traps H_2 and small products more efficiently, but at a cost of stronger guest–host interaction. Higher hydrides are formed more easily in neon because of more diffusion before solidification. Pure hydrogen or deuterium, of course, favors higher hydrides and typically provides frequencies between neon and argon matrix values. Normal hydrogen (F.P. 14.0 K) is more difficult to freeze than deuterium (F.P. 18.6 K) and both ortho and para nuclear spin isomers are present.

Density functional theoretical (DFT) calculations of transition metal hydrides and their hydrogen complexes were done for comparison. The Gaussian 98 program system[25] was employed to calculate the structures and frequencies of expected product molecules using the BPW91 and B3LYP density functionals. The 6–311++G(d,p) basis set for hydrogen and the LANL ECP plus DZ and SDD pseudo-potentials for transition metal atoms in Gaussian 98 were used.[25] All geometrical parameters were fully optimized and the harmonic vibrational frequencies were obtained analytically at the optimized structures. Such DFT calculations predict metal-hydride vibrational frequencies (usually a few % too high)[26] and are a great help in identifying new product species. Extensive computational studies for larger organometallic transition metal complexes have recently been reviewed and compared with experiment.[27]

3 Dihydrides

Metal dihydrides form two basic structures, the classical open dihydride MH_2 and the dihydrogen complex M(H_2). However, most metal atoms are sufficiently reactive to give the classical dihydride as will be discussed below.

3.1 MH_2 (M = Sc–Zn)

The first-row transition metal dihydrides were first investigated using thermal metal atom reactions[21–23,28,29] and then with laser-ablated metal atoms.[19,30–35] In general, the results are in agreement; however, thermal metal atoms usually require ultraviolet photolysis to activate dihydrogen whereas laser-ablated metal atoms are sufficiently energetic to react with dihydrogen during matrix sample deposition. Table 1 compares BPW91 calculated states, structures, and frequencies with argon matrix absorptions for first-row dihydrides. The small ScH_2 molecule was apparently not trapped in a recent investigation although YH_2 was observed.[30] The use of isotopic substitution for identifying a dihydride is illustrated in Fig. 2. Note that the two stretching modes of YHD at 1428.4 and

Table 1 Calculated states, bond lengths, angles, and stretching frequencies and argon matrix stretching frequencies observed for the first row transition metal dihydrides[a]

	ScH_2	TiH_2	VH_2	CrH_2	MnH_2	FeH_2	CoH_2	NiH_2	CuH_2	ZnH_2
Ground State	$^2A_1$	$^3A_1$	$^4B_2$	$^5B_2$	$^6A_1$	$^5A_1$	$^4B_2$	$^1A_1$	$^2B_2$	$^1\Sigma_g^+$
M–H (Å)	1.815	1.749	1.692	1.638	1.669	1.620	1.566	1.425	1.515	1.542
HMH (deg.)	116[b]	122	118	110	156[e]	146[f]	140	77	124	180
Calc. ν_3 (b_2)	1506	1578	1615	1663	1625	1694	1736	2119	1631	1908
Calc. ν_1 (a_1)	1528	1592	1639	1672	1691	1745	1800	2125	1770[i]	1900
Obs. ν_3 (b_2)		1435[c]	1508[c]	1614[d]	1592[e]	1661[f]	1684[g]	1969[h]		1870[j]
Obs. ν_1 (a_1)			1532	1651				2007		

[a] Calculated at the BPW91/6-311++G(d,p) level. [b] Ref. 30, B3PW91 functional. [c] Ref. 22. [d] Ref. 19. [e] Refs. 20,33. [f] Ref. 32. [g] Ref. 28. [h] Ref. 34. [i] Ref. 35. [j] Ref. 29.

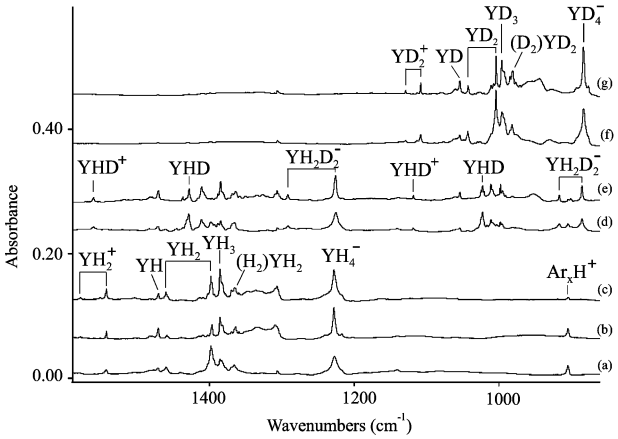

Fig. 2 Infrared spectra in 1590–860 cm^{-1} region for laser-ablated yttrium co-deposited with argon/hydrogen samples. (a) 5% H_2 in argon deposited at 3.5 K for 60 min, (b) after annealing to 16 K, (c) after $\lambda > 240$ nm photolysis for 15 min, (d) 5% HD in argon deposited at 3.5 K for 70 min, (e) after annealing to 16 K, (f) 5% D_2 in argon deposited at 3.5 K for 60 min, and (g) after annealing to 16 K. (Reprinted with permission from Ref. 30. Copyright 2002 American Chemical Society.)

1021.7 cm^{-1} are intermediate between the symmetric (a_1) and antisymmetric (b_2) stretching modes of YH_2 at 1459.8, 1397.8 cm^{-1} and of YD_2 at 1042.0, 1003.2 cm^{-1}. Thus, the H/D isotopic frequency ratios are 1.4010 and 1.3933 for the two modes.

The trends in Table 1 are noteworthy: First, the increasing H–M–H valence angle from ScH_2 to MnH_2 and FeH_2, which are probably linear,[32,33] is in agreement with recent LMR spectroscopy of FeH_2, which is the only transition metal dihydride to be investigated in the gas phase.[36] This trend can be explained by decreasing d character in the sd hybrid orbitals, which reaches zero d character in the pure sp hybrid for ZnH_2. Second, increasing frequencies follow a general decrease in metal–hydrogen bond length along the transition series. The acute angle $^1A_1$ ground state for NiH_2 may be an anomaly, but the identification of this state in solid argon by the Weltner group appears to be sound.[34] However, recent theoretical calculations show that the $^3\Delta_g$ state is close in energy, and gaseous NiH_2 might very well have the linear $^3\Delta_g$ ground state.[37]

Ozin and Gracie reported that the photochemical reaction of Cu (^2P) and H_2 gave CuH and H and that the back reaction produced Cu + H_2 and not CuH_2.[38] Although CuH_2 ($^2B_2$) is physically stable, it is 6 kcal mol^{-1} higher in energy than Cu + H_2, and any CuH_2 produced by excited Cu must be protected by a barrier to prevent decomposition. A 20 kcal mol^{-1} barrier has been predicted by Garcia-Prieto, *et al.*[39] and evidence for CuH_2 has very recently been found in solid hydrogen.[35] However, hydride anion and CuH combine to give the very stable linear CuH_2^- anion observed at 1497 cm^{-1} in solid argon.[35] The isoelectronic zinc dihydride molecule forms readily from the reaction of ^3P metastable excited zinc atoms with hydrogen in the argon matrix gas and exhibits a relatively high 1870 cm^{-1} H–Zn–H stretching frequency.[29]

3.2 MH_2 (M = Y–Cd)

The second-row transition metal dihydrides have been observed except for radioactive Tc, noble Pd which forms only the complex, and Ag.[18,23,29,30,40–43] The strong b_2 modes for the second-row dihydrides (Table 2) in solid argon (except where noted) are higher than their first row counterparts in all cases. This is particularly so for RuH_2 and RhH_2, where the second-row dihydrides are lower spin states. The RuH_2 molecule exhibits both a_1 and b_2 modes (at 2004 and 1984 cm^{-1} in solid neon),[42] and BPW91 calculations predict a bent (90.3°) $^1A_1$ ground state. Likewise, RhH_2 gives rise to both stretching modes (2053 and 2099 cm^{-1}, see Fig. 5), and BPW91 calculations find a bent (83.5°) $^2A_1$ ground state.[43]

3.3 MH_2 (M = La, Hf, W, Re, Pt, Au, Hg)

Laser-ablation has facilitated evaporation of the refractory metals, and seven of the third row transition metal dihydrides have been observed.[9,30,33,35,40,44,45] The strong b_2 modes for the third-row dihydrides (Table 3) are higher than their second-row counterparts. This is due to relativistic contraction not counterbalanced by shell expansion and is characteristic of relativistic effects for third row molecules.[46–48] Only the more intense bending mode has been observed in the Au case.

The initial reaction of H_2 and ground state Pt produced thermally in the Manceron laboratory proceeds on annealing in the argon matrix,[44] and you cannot get Pt atoms and H_2 molecules much colder. With the inclusion of spin–orbit coupling, triplet and singlet

Table 2 Calculated states, bond lengths, angles, and stretching frequencies and argon matrix stretching frequencies observed for the second row transition metal dihydrides[a]

	YH_2	ZrH_2	NbH_2	MoH_2	RuH_2	RhH_2	CdH_2
Ground State	$^2A_1$	$^3B_1$	$^4B_1$	$^5B_2$	$^1A_1$	$^2A_1$	$^1\Sigma_g^+$
M–H (Å)	1.955	1.863	1.783	1.713	1.558	1.531	1.683
HMH (deg.)	115	118	117	109	90	84	180
Calc. ν_3 (b_2)	1474	1608	1745	1819	2112	2156	1790[j]
Calc. ν_1 (a_1)	1518	1624	1727	1830	2164	2207	1794
Obs. ν_3 (b_2)	1398[b]	1524[c]	1569[d]	1719[e,f]	1984[g,h]	2053[g,i]	1754[j]
Obs. ν_1 (a_1)	1460				2004	2099	

[a] Calculated at the BPW91/6-311++G(d,p) level. [b] Ref. 30, B3PW91 functional. [c] Ref. 40. [d] Ref. 18. [e] Ref. 41. [f] Ref. 23 reports 1709 cm^{-1} in solid krypton. [g] Neon matrix. [h] Ref. 42. [i] Ref. 43. [j] Ref. 29, CCSD(T).

Table 3 Calculated states, bond lengths, angles, and stretching frequencies and argon matrix stretching frequencies observed for the third row transition metal dihydrides[a]

	LaH_2	HfH_2	WH_2	ReH_2	PtH_2	AuH_2	HgH_2
Ground State	$^2A_1$	$^3B_1$	$^5B_2$	$^6A_1$	$^1A_1$	$^2B_2$	$^1\Sigma_g^+$
M–H (Å)	2.104	1.865	1.717	1.745	1.521	1.619	1.642
HMH (deg.)	109	119	113	146	86	129	180
Cal. ν_3 (b_2)	1356	1632	1922	1718	2427	1758[g]	1920[h]
Calc. ν_1 (a_1)	1389	1661	1928	1874	2459	2004[g]	2044
Obs. ν_3 (b_2)	1283[b]	1622[c]	1832[d]	1646[e]	2349[f]		1895[i]
Obs. ν_1 (a_1)					2366		

[a] Calculated at the BPW91/6-311++G(d,p) level. [b] Ref. 30, B3PW91 functional. [c] Ref. 40, B3PW91 functional. [d] Ref. 13. [e] Ref. 33. [f] Ref. 44. [g] Ref. 53: calculated intensities < 2 km mol^{-1}. [h] Ref. 29, CCSD(T). [i] Ref. 45.

Pt atomic states mix in the curve crossing region, and ground state Pt reacts spontaneously to form PtH_2 in the $^1A_1$ state.[49,50] This mechanism is corroborated by a very recent theoretical investigation.[51]

$$Pt(^3D_3) + H_2\ (^1\Sigma^+) \rightarrow PtH_2\ (^1A_1)\ \Delta E = -50\ \text{kcal mol}^{-1} \quad (1)$$

The AuH_2 molecule is particularly interesting because the CuH_2 and AgH_2 molecules could not be prepared in the Ozin resonance photolysis work.[38] However, it is known that, owing in part to relativistic effects, the AuH bond is stronger than the AgH and CuH bonds,[52] so AuH_2 has a better chance of surviving a resonance photolysis experiment. Manceron has succeeded in preparing $(H_2)AuH$ and AuH_2 from the resonance photolysis of Au in solid hydrogen,[35] and the AuH_2 molecule is characterized by its strong bending mode at 638 cm^{-1}.[53] Laser-ablation experiments also produced AuH_2, AuHD, and AuD_2. Balusubramanian and Liao calculated that the AuH_2 molecule is separated by a 20 kcal mol^{-1} barrier from its some 20 kcal mol^{-1} lower energy precursor-decomposition products Au + H_2.[54]

The HgH_2 molecule is also a unique dihydride.[45] Ground state Hg (^1S) is a closed-shell unreactive atom, but the Legays have shown that the triplet state Hg (^3P) inserts spontaneously into dihydrogen. The linear molecule has a strong 1895.8 cm^{-1} antisymmetric stretching frequency in solid argon, which is higher (+25 cm^{-1}) than the analogous mode in ZnH_2. The Legays also used an argon overcoat to retain H_2 condensed at 5.7 K and measured HgH_2 at 1902.7 cm^{-1} in solid hydrogen.

3.4 $Pd(H_2)$

Palladium hydrogen complexes were first observed by Ozin and Garcia-Prieto in solid krypton and xenon, and the spectra were interpreted in terms of both side and end-bonded complexes.[8] However, subsequent theoretical investigations find a stable minimum only for the side-bonded structure, and new experimental evidence indicates reassignment of PdHH features to $Pd(H_2)_2$.[9] The $Pd(H_2)$ complex was characterized by 960 cm^{-1} and split 894, 885 cm^{-1} stretching modes in solid krypton and xenon, respectively,[8] and these are in accord with the more recent 950 cm^{-1} argon matrix observation.[9]

A large yield of $Pd(H_2)$ was prepared with thermal Pd atoms, and new absorptions were observed at 950, 1507, and 2971 cm^{-1} in solid argon in the Manceron laboratory in Paris.[9] These bands show appropriate HD and D_2 isotopic shifts for assignment to $Pd(H_2)$. In fact the low $Pd(H_2)/Pd(D_2)$ (950/714 = 1.311) isotopic frequency ratio indicates significant anharmonicity in the Pd–(H_2) potential function. The 2971 band is due to the H–H stretching mode (a_1), the 1507 cm^{-1} absorption arises from the antisymmetric (b_2) Pd–H_2 stretching mode, and the strong 950 cm^{-1} band is assigned to the symmetric (a_1) Pd–H_2 stretching vibration. These bands are compared in Table 4 with vibrational frequencies calculated at the DFT level of approximation: agreement is very good but not perfect. The $Pd(H_2)$ stretching frequencies are in the ranges reported for these modes in transition metal–(H_2) complexes.[1–3,6] The analogous modes for the $(PCy_3)_2W(CO)_3(H_2)$ complex are 953, 1575, and 2690 cm^{-1}. The H–H stretching mode for $Pd(H_2)$ in solid argon, 2971 cm^{-1}, is between the 3030, 3080 and 2711 cm^{-1} values, respectively, for the Cr, Mo, $W(CO)_5(H_2)$ complexes in liquid xenon.[12]

Table 4 Observed argon matrix and calculated frequencies for $Pd(H_2)$

Observed[a]	Calculated[a]	Mode
2971 (16)[b]	2935 (83)[c]	ν_1 (a_1), H–H str
1507 (2)	1444 (8)	ν_3 (b_2), asym Pd–H_2 str
950 (360)	966 (170)	ν_2 (a_1), sym Pd–H_2 str

[a] B3LYP/6-311++G(2d, 2p)/SDD, Ref. 9. [b] Relative integrated intensities. [c] Calculated infrared intensities, km mol^{-1}.

Bonding between the Pd and H_2 subunits was investigated by Alikhani *et al*. using the natural bonding orbital method.[9] Occupancy of the σ bonding orbital of the H_2 molecule decreased slightly on going from free H_2 to the Pd–H_2 complex (2 e *versus* 1.9 e), which is in line with weakening of H–H bonding upon complexation. In addition, no bonding orbital was found between the palladium atom and dihydrogen molecule. The effective charge transfer from metal to ligand was calculated to be only 0.06 e. From the NBO analysis, the σ donation (from H_2 to the vacant 5s orbital of Pd) and π back-donation (from the filled 4d orbital of Pd to the dihydrogen σ* orbital) were found to be 0.17 and 0.23 e, respectively. Therefore, the interaction between Pd and H_2 arises from two cooperatively coupled intermolecular donor–acceptor delocalizations that lead to minor charge reorganization, and the spontaneous reaction (2) forms the dihydrogen complex.

$$Pd(^1S_o) + H_2(^1\Sigma_g^+) \rightarrow Pd(H_2)\ (^1A_1)\ \Delta E = -18\ \text{kcal mol}^{-1} \quad (2)$$

The differences in the noble metals Pd and Pt and their hydrides come back to their d^{10} and d^9s electronic configurations. The ground state metals from thermal evaporation react spontaneously to form the $Pd(H_2)$ dihydrogen complex and the PtH_2 classical dihydride, respectively.[8,9,44] Fig. 3 illustrates the spectra of $Pd(H_2)_{1,2,3}$ complexes, and Fig. 4 compares their computed structures with that for PtH_2. The strong Pd–(H_2) stretching frequency at 950 cm^{-1} and the a_1 and b_1 Pt–H modes at 2366, 2349 cm^{-1} are diagnostic of these structures and bonding models. The

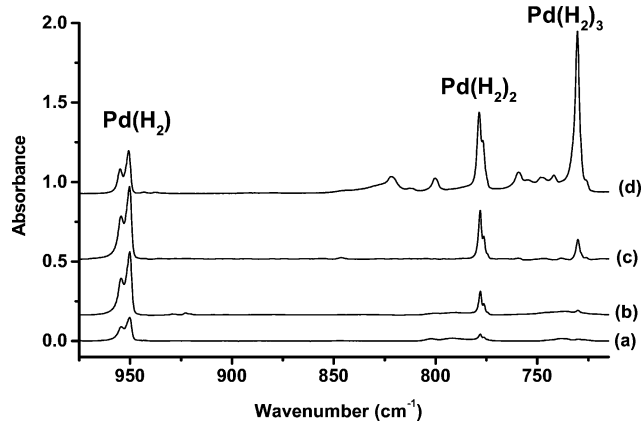

Fig. 3 Infrared spectra of products formed by the reaction of thermal Pd atoms co-deposited for 90 min with H_2 in excess argon at different concentrations. (a) $Pd/H_2/Ar$ = 0.5/2/100, (b) $Pd/H_2/Ar$ = 0.6/4/100, (c) $Pd/H_2/Ar$ = 0.3/8/100 and (d) $Pd/H_2/Ar$ = 0.3/24/100. (Reprinted with permission from Ref. 9. Copyright 2001 American Chemical Society.)

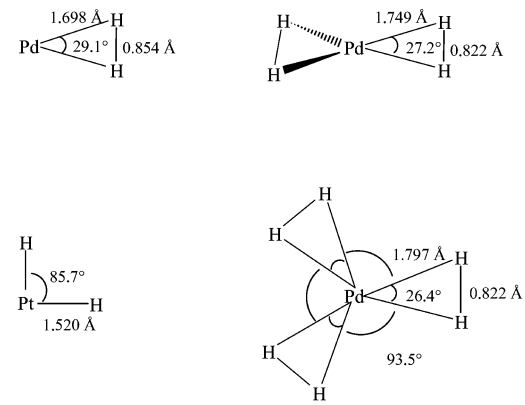

Fig. 4 Structures calculated for PtH_2, $Pd(H_2)$, $Pd(H_2)_2$, and $Pd(H_2)_3$ using B3LYP/6-311++G(d,p)/SDD. Angles in degrees and distances in Ångstroms.

analogous open PdH_2 dihydride state computed to be 5.0 kcal mol^{-1} higher in energy than $Pd(H_2)$ is not observed.[9]

Three further points about $Pd(H_2)$ are of considerable chemical interest. First, $Pd(H_2)$ adds one and two more dihydrogen ligands to form the $Pd(H_2)_2$ and $Pd(H_2)_3$ complexes, which will be discussed later. Second, one more Pd atom can activate the dihydrogen ligand and form the open rhombus structure, $Pd(\mu\text{-}H)_2Pd$, which absorbs at 1348 cm^{-1} in the infrared spectrum. Third, electron capture allows one Pd to activate dihydrogen to form the PdH_2^- anion.[9]

3.5 Dihydride anions and comparisons

Dihydride anions have been investigated in the gas phase by photoelectron (photodetachment) spectroscopy.[55] These transition metal dihydride anions are typically prepared by electrical discharge methods and mass selected before laser photodetachment.

With laser ablated Pd, a sharp new absorption at 1247.0 cm^{-1} shifts to 908.5 cm^{-1} with D_2. New bands at 1479.5 and 981.8 cm^{-1} are found with the HD reagent. Companion DFT calculations predict the $^2\Sigma_g^+$ state of linear $(HPdH)^-$ to have an extremely high intensity antisymmetric stretching fundamental near 1300 cm^{-1}. This facilitates identification of the linear $HPdH^-$ anion in solid argon, which is formed through electron capture by $Pd(H_2)$. Clearly, the extra electron helps Pd to reduce H_2 and to form stronger Pd–H bonds.

This is a genuine $Pd(I)H_2^-$ molecular anion isolated in solid argon, in contrast to the ternary $Na_2[Pd(0)H_2]$ solid compounds prepared by reaction of NaH with palladium sponge at very high hydrogen pressure.[56,57] The out-of-phase frequency of the linear solid state PdH_2^{2-} anion (1455 cm^{-1}) with two adjacent Na^+ cations is higher than the argon matrix value for isolated PdH_2^- (1247 cm^{-1}).[9,57] Higher ternary hydrides such as $Na_2[Pd(II)H_4]$ have also been formed at very high hydrogen pressures,[57,58] although such dianions cannot be observed isolated in solid argon due to coulombic instability.

4 Trihydrides

Metal trihydrides are more difficult to characterize than dihydrides, and therefore, fewer cases are known. Examples of the classical trigonal form and the monohydride–dihydrogen complex will be considered next.

4.1 MH_3 (M = Sc, Y, La)

Laser-ablated Group 3 atoms react with H_2 to form the monohydride diatomic molecules and with another H_2 to form the trihydride molecules.[30] The ν_3 (e) modes for the three Group 3 trihydrides are 1487.7, 1385.1, and 1263.6 cm^{-1} (YH_3 is shown in Fig. 2). These bands exhibited H/D isotopic frequency ratios of 1.379, 1.392, and 1.397, respectively, as the increasing metal mass increases the H(D) contribution to the vibrational mode. Experiments with HD produced triplet bands in the M–H and in the M–D regions, which are the characteristic MH_2D and MHD_2 mixed isotopic pattern. Accompanying BPW91 functional calculations predict trigonal almost planar MH_3 molecules with strong e modes, which require 0.980, 0.960, and 0.957 scale factors to fit the observed argon matrix frequencies. This structure for ScH_3 is in agreement with recent CCSD(T) calculations of Balbanov and Boggs.[59]

$$Sc + H_2 \rightarrow ScH + H \quad (3)$$

$$H_2 + ScH \rightarrow ScH_3 \quad (4)$$

4.2 $(H_2)MH$ (M = Fe)

Group 8 tends to form lower hydrides. The dominant product with iron is FeH_2 at 1661 cm^{-1} in solid argon, 1675 cm^{-1} in solid neon, and 1666 cm^{-1} in solid hydrogen:[32,42] FeH_2 has a 1675 cm^{-1} gas phase fundamental.[36] Note that the neon matrix most closely approximates the gas phase and that the hydrogen matrix value is between neon and argon matrix values. The second most intense absorption is at 1653, 1729, and 1714 cm^{-1} for these three matrices, respectively. The trigonal FeH_3 ground state has been reported as $^6A_1'$ at the CCSD(T) level of theory;[59] however, we find the $^4B_2$ state $(H_2)FeH$ complex to be 26 kcal mol^{-1} lower in energy using the BPW91 density functional. Hence, $(H_2)FeH$ and not FeH_3 is trapped in the matrix. The strong Fe–H mode in $(H_2)FeH$ is calculated to fall 6 cm^{-1} below that for $^4\Delta$ FeH and 29 cm^{-1} above $^5A_1$ FeH_2. The 1729 and 1714 cm^{-1} bands in solid neon and hydrogen are assigned to the $(H_2)FeH$ complex.

4.3 $(H_2)RhH$ and RhH_3

Rhodium covers the entire range of possibilities. The argon matrix spectrum of Rh and H_2 reveals absorptions at 2053.4 and 1920.6 cm^{-1} for RhH_2 and RhH, respectively (Fig. 5). Annealing produces

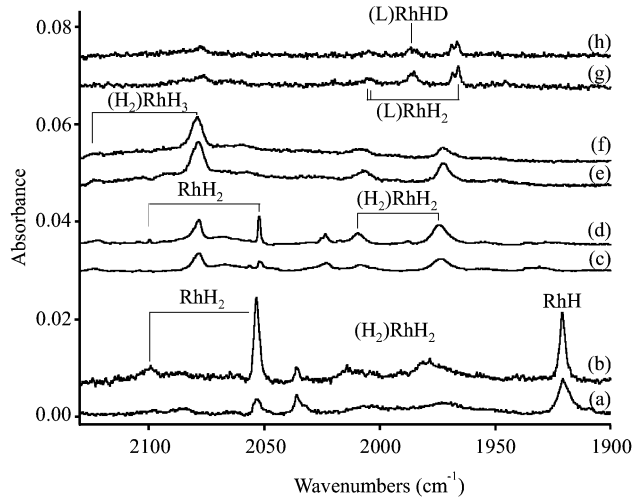

Fig. 5 Infrared spectra in the 2130–1900 cm^{-1} region for laser-ablated Rh co-deposited with H_2 in different matrices. (a) 2% H_2 in argon after deposition at 7 K for 60 min, (b) after annealing to 30 K, (c) 2% H_2 in neon after deposition at 3.5 K for 60 min, (d) after annealing to 11 K, (e) pure n-H_2 after deposition at 3.5 K for 30 min, (f) after annealing to 6.5 K and $\lambda >$ 240 nm photolysis, (g) 50% H_2 + 50% D_2 after deposition at 3.5 K for 30 min, and (h) after annealing to 6.5 K and $\lambda >$ 240 nm photolysis.

a new band at 2014.0 cm^{-1} for $(H_2)RhH$ at the expense of RhH and increases the 2053.4 cm^{-1} band and a weaker associated 2099.4 cm^{-1} absorption.[43] The latter is due to the ν_1 (a_1) mode of RhH_2 ($^2A_1$) and the former to the ν_3 (b_2) mode. Although calculations predict that RhH_3 (C_{3v}, $^1A_1$) is 27 kcal mol^{-1} more stable than $(H_2)RhH$ (C_{2v}, $^3A_1$), only the latter is observed in solid argon. However, additional absorptions are observed for the $(H_2)RuH_3$ and $(H_2)RhH_2$ complexes in solid neon at 2078.2 and 1974.2 cm^{-1}, respectively.[43] These higher complexes, computed to be bound by 8 kcal mol^{-1}, are favored in pure hydrogen. Fig. 5 compares the Rh + H_2 reaction products in argon, neon, and hydrogen matrices and illustrates the effect of reagent diffusion and concentration on the co-deposition reactions.

These isolated rhodium hydride molecule frequencies fall in the 2150–1900 cm^{-1} range for organometallic rhodium hydride complex $HRh(L)_4$ absorptions.[60–62] For example the $HRh(PPh_3)_4$ complex exhibits a 2140 cm^{-1} Rh–H stretching mode (H/D ratio 1.390) in a KBr disc.[62] Thus it appears that the Rh–H stretching frequency increases upon coordination at the Rh center by H_2 and by PR_3 ligands, and that the Rh–H stretching frequency can be "tuned" by changing the ligand. The situation is, however, more complicated for $RuH_2(PR_3)_4$ complexes. A 2080 cm^{-1} Ru–H stretching frequency has been reported for the R = Ph compound with a presumed *trans*-dihydride structure,[62] but two frequencies at 1940 and 1885 cm^{-1} (H/D ratios 1.396 and 1.391) have been observed for the diphenylmethylphosphine complex, which is assumed to have the *cis*-dihydride structure.[61] The naked RuH_2

molecule in solid neon exhibits higher 2004 and 1984 cm^{-1} frequencies and the computed $^3B_1$ ground state RuH_2 molecule is bent (99°).[42]

$$Rh + H_2 \rightarrow RhH_2 \quad (5)$$

$$H_2 + RhH_2 \rightarrow (H_2)RhH_2 \quad (6)$$

$$H_2 + RhH_3 \rightarrow (H_2)RhH_3 \quad (7)$$

4.4 $(H_2)MH$ and $(H_2)AuH_3$ (M = Cu, Ag, Au)

Gold hydride is a stable diatomic molecule, which has been characterized by electronic band spectroscopy in the gas phase,[52] but there is no evidence for stable, solid gold hydrides.[63] Although mononuclear gold hydride complexes are unstable or unknown,[64] gold hydrides have been observed in heterobimetallic complexes with ruthenium, iridium, and platinum.[65–67] The anticipated AuH_3 molecule has been the subject of several theoretical investigations. Gold trihydride was first predicted to be T-shaped from non-relativistic and relativistic pseudo-potential calculations.[48] Very recent quantum chemical calculations[68,69] show that the Y-shaped $(H_2)AuH$ complex is more stable than the T-shaped AuH_3 form. Other very recent effective core potential calculations show that AuH_3 is a transition state with an imaginary b_1 bending frequency and agree that $(H_2)AuH$ is the stable equilibrium structure.[70] Gold is also interesting because it forms unusually strong chemical bonds due to relativistic effects.[46–48,71]

Laser-ablated coinage metal atom reactions with H_2 in excess argon, neon, and pure hydrogen give the MH diatomic and/or $(H_2)MH$ dihydrogen complex for all metals.[35,72] The 2226.6 or 1597.2 cm^{-1} bands observed with laser-ablated gold atoms and H_2 or D_2 in solid argon are slightly blue shifted from the 2218.8 or 1591.7 cm^{-1} fundamentals deduced for AuH or AuD from electronic band spectra.[52] Both data sets have the 1.394 H/D frequency ratio, which is appropriate for a heavy metal hydride vibration.

In addition, a sharp 2173.6 cm^{-1} band appears and increases on annealing to allow diffusion of H_2 at the expense of AuH, and a 1559.3 cm^{-1} band increases on annealing to allow reaction of D_2 at the expense of AuD. Our DFT calculations (BPW91) predict the strongest Au–H stretching mode for $(H_2)AuH$ to be 56.8 cm^{-1} below AuH and with greater infrared intensity. The H/D frequency ratio 1.394 is the same as for AuH/AuD. Assignment of these bands to the Au–H stretching mode of the stable $(H_2)AuH$ complex is further substantiated by observation of the strong 1556.5 cm^{-1} and two weaker fundamentals in the pure deuterium matrix where the yield of $(D_2)AuD$ is increased owing to the effectively high concentration of the D_2 reagent (Fig. 6(c)).[72] Unfortunately the D–D stretching mode was too weak to be observed.

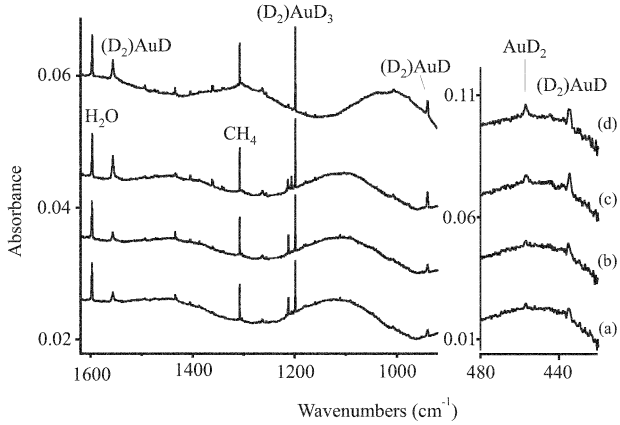

Fig. 6 Infrared spectra of products of laser-ablated gold and deuterium reactions in pure deuterium frozen at 3.5 K. (a) Gold atoms co-deposited with pure deuterium for 25 min, (b) after annealing to 7 K, (c) after $\lambda > 240$ nm irradiation, and (d) after annealing to 8 K.

Hydrogen matrix experiments with Cu and Ag produce the analogous $(H_2)CuH$ and $(H_2)AgH$ complexes, which exhibit H–H stretching modes at 3567 and 3806 cm^{-1} and M–H stretching vibrations at 1861 and 1743 cm^{-1}, respectively.[35] Note that these H–H stretching modes for Group 11 $(H_2)MH$ complexes are higher than that for $Pd(H_2)$ and for the Group 6 carbonyl $M(CO)_5(H_2)$ complexes.[9,12] Hence, the coinage metal complexes involve a weaker interaction with the H_2 ligand.

A new 1661.5 cm^{-1} band in pure hydrogen and the strong, sharp 1198.6 cm^{-1} absorption in pure deuterium are in reasonable agreement with the DFT prediction of a very strong antisymmetric (b_1) H–Au–H stretching mode for AuH_3, and AuD_3. However, AuH_3 is less stable than $(H_2)AuH$, and AuH_3 is a transition state with an imaginary b_1 antisymmetric bending mode. Calculations were performed to search for a stable complex of AuH_3 that might match the observed spectrum: $(H_2)AuH_3$ is stable to dissociation into H_2 and AuH_3 (8 kcal mol^{-1}, B3LYP) but higher energy than $H_2 + (H_2)AuH$ (23 kcal mol^{-1}, B3LYP). Once formed from AuH_3* and H_2, there is apparently a considerable energy barrier for $(H_2)AuH_3$ to eliminate H_2.[72]

The three Au–H stretching modes in the AuH_3 transition state are changed little in the stable $(H_2)AuH_3$ complex, but the imaginary b_1 bending frequency involving the unique, short Au–H bond is real in $(H_2)AuH_3$ using the BPW91 and B3LYP functionals. Thereby the AuH_3 transition state is stabilized through complexing to dihydrogen. An experiment with pure HD gives a mixed H,D isotopic pattern that confirms the C_{2v} T-shaped structure for the AuH_3 subunit.

The coinage metal hydride products observed in argon, neon, and hydrogen matrices are summarized in Table 5.

Table 5 Coinage metal hydride products in argon, neon, and hydrogen matrices

Argon	Neon	Hydrogen
CuH	CuH	CuH_2
$(H_2)CuH$	$(H_2)CuH$	$(H_2)CuH$
AgH	—	—
$(H_2)AgH$	$(H_2)AgH$	$(H_2)AgH$
AuH	$(H_2)AuH$	$(H_2)AuH$, AuH_2
$(H_2)AuH$	$(H_2)AuH_3$	$(H_2)AuH_3$

5 Tetrahydrides

Tetrahydrides include the classical form and the dihydrogen metal dihydride complex.

5.1 MH_4^- (M = Sc, Y, La)

Group 3 metals are isoelectronic in the valence shell with Group 13 metals where stable tetrahydrometallate anions (AlH_4^-) are well known. Laser-ablated scandium family metals activate dihydrogen as MH_2 dihydrides, which readily complex with another dihydrogen to form $(H_2)MH_2$ complexes. This is shown in Fig. 2(a),(b) where annealing to 16 K increases $(H_2)YH_2$ at the expense of YH_2, and subsequent UV photolysis, Fig. 2(c), regenerates YH_2. The latter complexes have substantial (2.8–2.4 eV) computed electron affinities, and the tetrahedral MH_4^- anions are formed in the laser-ablation process.[73] New 1227.3 and 882.3 cm^{-1} bands were assigned to antisymmetric Y–H and Y–D stretching fundamentals ν_3 (t_2) of the tetrahedral anions YH_4^- and YD_4^- based on the following evidence. In the HD experiments the above bands split into 1291.4 and 1225.4 cm^{-1} and 915.7 and 884.5 cm^{-1} doublets, respectively, on symmetry lowering, which are due to symmetric and antisymmetric YH_2 and YD_2 stretching fundamentals in $YH_2D_2^-$. The antisymmetric YH_2 and YD_2 modes in $YH_2D_2^-$ are very close to the ν_3 (t_2) modes observed in YH_4^- and YD_4^-, respectively, and the new symmetric modes lie higher about 64 cm^{-1} for the YH_2 mode and 33 cm^{-1} for the YD_2 mode in the $YH_2D_2^-$ anion. This pattern of four Y–H(D) stretching modes for

$YH_2D_2^-$ verifies a tetrahydride species.[73] Note that the Ar_xH^+ and Ar_xD^+ species are observed in these experiments at 903.3 and 643.3 cm^{-1}, respectively, which provides for a charge balance in the matrix.[74,75] The antisymmetric M–H stretching mode ν_3 (t_2) decreases from 1305.1 cm^{-1} for ScH_4^- to 1227.3 cm^{-1} for YH_4^- and to 1114.1 cm^{-1} for LaH_4^- suggesting a straightforward metal–hydrogen bond length increase from ScH_4^- to YH_4^- and to LaH_4^-, respectively, which is in line with DFT computations. Finally, the strong degenerate ν_3 (t_2) mode computed for YH_4^- at 1241.3 cm^{-1} and YD_4^- at 886.0 cm^{-1} are in excellent agreement with observed values.[73]

The anion identification is further confirmed with CCl_4 additive, which serves as an electron trapping agent.[17] The elimination of YH_4^- with CCl_4 in the sample is due to the preferential capture of ablated electrons by CCl_4. Hence, YH_4^- is identified from the observation of four Y–H(D) stretching absorptions on HD substitution, agreement with DFT frequency calculations, and CCl_4 doping to verify the anion charge.[73]

5.2 MH_4 (M = Ti, Zr, Hf)

The Group 4 tetrahydrides are formed through the spontaneous reaction of MH_2 with another H_2. The TiH_4 molecule was first prepared by the photochemical reaction of thermally evaporated Ti and $2H_2$ in the Margrave laboratory and then by laser-ablated Ti atom reactions with H_2 in excess argon.[22,31] These tetrahydrides are identified from four bond stretching vibrations for the MH_2D_2 molecules.[40] The isoelectronic TiH_4, ZrH_4, and HfH_4 molecules exhibit ν_3 (t_2) modes at 1663.8, 1623.6 and 1678.4 cm^{-1}, respectively, in solid argon. The increase in frequency from ZrH_4 to HfH_4 has been attributed to the relativistic bond-length contraction predicted for HfH_4 (1.907 Å) relative to ZrH_4 (1.912 Å).[46] However, La and Hf are separated by the 14 elements of the lanthanide series, and no such contraction occurs for La relative to Y as is described above.

5.3 $(H_2)CrH_2$, MoH_4, and WH_4

The Group 6 tetrahydrides provide a contrast: Fig. 7 compares Cr, Mo, and W reaction products with H_2 in excess neon. First, CrH_4 is

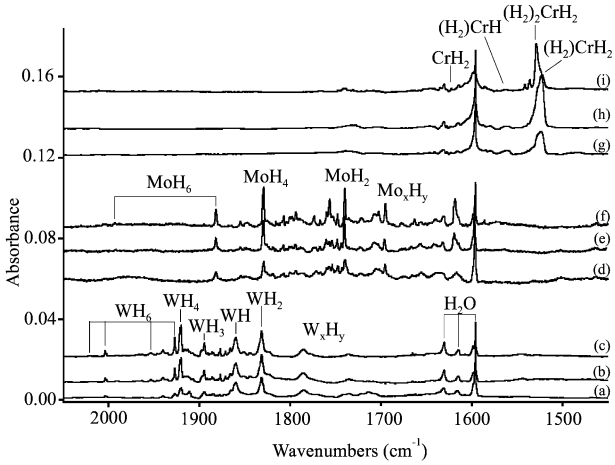

Fig. 7 Infrared spectra in the 2050–1450 cm^{-1} region for laser-ablated Group 6 metal atoms reacted with H_2 during freezing in excess neon at 3.5 K. (a) W and 4% H_2 co-deposited for 1 h in neon, (b) after annealing to 10 K, (c) after annealing to 11 K, (d) Mo and 4% H_2 co-deposited for 1 h in neon, (e) after annealing to 9 K, (f) after annealing to 11 K, (g) Cr and 5% H_2 co-deposited for 1 h in neon, (h) after $\lambda > 290$ nm photolysis for 10 min, and (i) after annealing to 12 K.

most stable in the C_{2v} $(H_2)CrH_2$ structure and $^5A_1$ state,[76] although isotopic scrambling occurs in these experiments on deposition and on ultraviolet photolysis through the $^3A_1$ tetrahedral excited state,[19] as is illustrated in Scheme 1. Using mixed $H_2 + D_2$ both pure and diluted in neon, the $(H_2)CrD_2$ and $(D_2)CrH_2$ species are major and the $(HD)_2CrHD$ species is a minor deposition product, and all

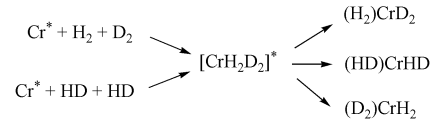

Scheme 1

increase on annealing and photolysis.[19] Such rearrangements are in accord with dihydrogen–dihydride exchange processes in organometallic metal hydride, dihydrogen complexes, which have been reviewed by Eisenstein, *et al.*[27] The diagnostic frequency for $(H_2)CrH_2$, 1526 cm^{-1} in solid neon, is 102 cm^{-1} lower than for CrH_2, 1628 cm^{-1}, which is due in part to a substantial change in the H–Cr–H angle.[14] This means that the absorption first assigned to CrH_3 by the Margrave group is, in fact, due to $(H_2)CrH_2$.[19,23] Second, MoH_4 and WH_4 are most stable in the tetrahedral $^3A_1$ states characterized by ν_3 (t_2) modes at 1830 and 1920 cm^{-1} in solid neon, respectively.[13,41] Note that the W–H stretching frequencies are substantially higher than such Cr–H modes: Again the role of relativistic contraction is manifested.[46]

Tungsten is particularly difficult to evaporate, and laser-ablation is up to the task. Infrared spectra for laser-ablated W co-deposited with 4% H_2 in neon are shown in Fig. 8. The lowest three W–H

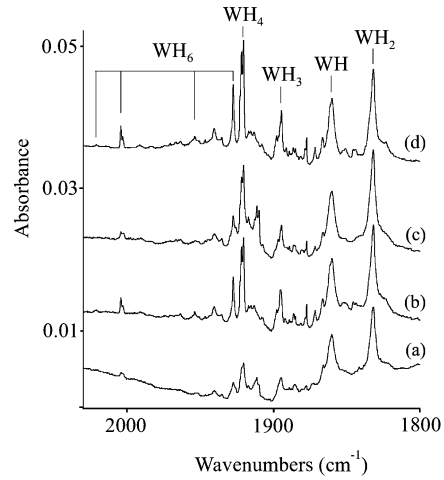

Fig. 8 Infrared spectrum in the W–H stretching region for tungsten hydrides prepared by reacting laser-ablated W atoms and H_2 in excess neon during co-deposition at 3.5 K. (a) W and 4% H_2 co-deposited for 1 h in neon, (b) after annealing to 10 K, (c) after broadband photolysis for 15 min, and (d) after annealing to 11 K. (Reprinted with permission from Ref. 13. Copyright 2002 American Chemical Society.)

stretching absorptions at 1895.3, 1860.2, and 1831.9 cm^{-1} are due, respectively, to the WH_3, WH, and WH_2 molecules. The W–H stretching mode for the $CpW(CO)_3H$ complex is at 1845 cm^{-1}, hence the isolated tungsten hydride molecules are good models for tungsten hydride bonds in ligated organometallic complexes.[13,77] The strongest band at 1920.5 cm^{-1} after annealing and photolysis is due to WH_4. This band shifts to 1377.0 cm^{-1} with D_2 (1.3947 ratio), and HD substitution gives four bands at 1935.8, 1920.2, 1384.8, and 1378.0 cm^{-1} for WH_2D_2, which shows that a tetrahydride is formed.[13]

5.4 $(H_2)RhH_2$ and $Rh(H_2)_2$

The above discussion of RhH_2 and RhH_3 included the $(H_2)RhH_2$ complex, which appears below isolated RhH_2 in the neon matrix spectrum (Fig. 5). BPW91 calculations predict 127, 142 cm^{-1} red-shifts for the dihydrogen complex from isolated RhH_2 and 78, 90 cm^{-1} red-shifts are observed in solid neon.[43] It is interesting to note that the H_2, D_2, and HD isotopic modifications of $(H_2)RhH_2$ interconvert on photolysis, which suggests that a tetrahedral $[RhH_2D_2]^*$ excited state is formed on photoexcitation. This is in accord with dynamic rearrangement processes for classical and nonclassical transition metal polyhydride complexes, which have

been explored experimentally and theoretically.[27] This rearrangement is illustrated in Fig. 5(g) where the complex prepared from H_2 + D_2 includes (HD)RhHD. Note also that the (L)RhH_2 complex bands are split as L can be H_2 and D_2 in this experiment.

In addition a weaker 738 cm^{-1} band increases on annealing, decreases on photolysis, and increases on final annealing, but these changes are small compared to those for (H_2)RhH_2, which is calculated to be more stable by 9 kcal mol^{-1} than the Rh(H_2)$_2$ isomer.[43] Our calculations further predict a very strong Rh–(H_2) stretching mode at 723 cm^{-1} for Rh(H_2)$_2$. The 738 cm^{-1} band shifts to 565 cm^{-1} with D_2 (H/D ratio 1.306) and exhibits a new 616 cm^{-1} intermediate component suggesting two equivalent H_2 ligands. With HD the band appears at 630 cm^{-1}, but photolysis decreases the 630 cm^{-1} band in favor of the 616 cm^{-1} absorption. Hence, photolysis initiates scrambling of Rh(HD)$_2$ and Rh(H_2)(D_2), and again suggests that a tetrahedral [RhH_2D_2]* intermediate is involved in the rearrangement process.

5.5 Pd(H_2)$_2$

The bisdihydrogen palladium complex (Fig. 3) gives rise to a strong (e) antisymmetric (H_2)–Pd–(H_2) mode at 778 cm^{-1}, which is intermediate between Pd(H_2) and Pd(H_2)$_3$ modes.[9] Note the proximity of the strong modes for the Rh(H_2)$_2$ and Pd(H_2)$_2$ bisdihydrogen complexes.

The results of a topological analysis on the Pd(H_2)$_{1,2,3}$ complexes show a substantial increase in charge flow to hydrogen, indicating a dominant d $\rightarrow$ σ* charge transfer interaction. In the Pd(H_2)$_{2,3}$ complexes the ligand effects on the Pd charge are additive, which leads to an electron population depletion so close to unity that further coordination higher than Pd(H_2)$_3$ is unfavorable.[9]

6 Hexahydrides

Metal hexahydrides range from trisdihydrogen complexes to classical hexahydrides.

6.1 Pd(H_2)$_3$

The trisdihydrogen palladium complex is formed through the addition of two H_2 molecules to Pd(H_2). Clearly higher hydrogen concentrations and the pure hydrogen matrix favor the tris complex. The strong doubly-degenerate Pd–(H_2) stretching mode is observed at 730 cm^{-1} in solid argon (Fig. 3). An even stronger in-plane ligand bending mode at 320 cm^{-1} in solid argon is more sensitive to mixed isotopic substitution. With H_2 + D_2 this band gives rise to new 317 and 270 cm^{-1} bands for Pd(H_2)$_2$(D_2) and to new 294 and 237 cm^{-1} bands for Pd(H_2)(D_2)$_2$, which verifies the doubly-degenerate nature of the mode and the tris-dihydrogen stoichiometry.[9] Manceron has shown that Pd(H_2)$_3$ is essentially the only product formed when thermal Pd atoms are condensed with pure normal H_2 near 3 K.[78] Palladium is the only metal that forms a tris-dihydrogen complex.

Although DFT calculations failed to converge under D_{3h} symmetry, C_{2v} symmetry revealed structural agreements consistent with the higher symmetry (Fig. 4). The Pd(HD)$_3$ complex retains double degeneracy when all HD subunits are oriented the same way in the molecular plane, but when one HD is turned opposing the other two, this degeneracy is split. Hence, the novel Pd(H_2)$_3$ complex is definitively identified through mixed isotopic spectra.[9]

6.2 (H_2)$_2$CrH_2, MoH_6, and WH_6

Theoretical calculations agree that the octahedral MH_6 structures predicted by VSEPR are considerably higher energy than lower symmetry structures.[14,15,27] For WH_6, an eclipsed distorted trigonal prism (C_{3v}) and for (H_2)$_2$CrH_2 a bis-dihydrogen complex (C_{2v}) are the computed global minima (Fig. 9), in $^1A_1$ and $^5A_1$ states, respectively.[13–15,19]

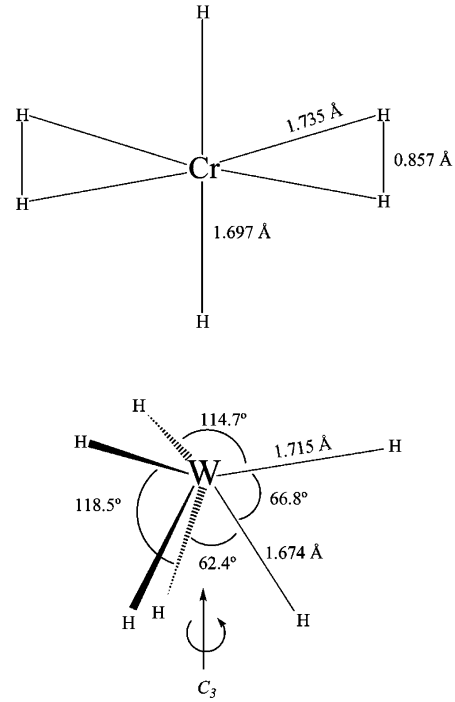

Fig. 9 Planar C_{2v} structure for (H_2)CrH_2(H_2) and distorted trigonal prismatic C_{3v} structure for WH_6 calculated using BPW91/6-311++G(d,p)/SDD.

The Cr/H_2/Ne system reveals a weak b_2 stretching mode at 1627.7 cm^{-1} for CrH_2 and the (H_2)CrH_2 complex shifted to 1525.8 cm^{-1}. Further annealing increases markedly a sharp 1529.5 cm^{-1} absorption that is assigned to the b_2 mode of linear CrH_2 in the bis-dihydrogen CrH_2 complex, which is the most stable form computed for CrH_6.[19] It has been suggested that DFT underestimates the interaction between the dihydrogen ligand and the metal complex.[27]

In addition Fig. 7 reveals two sharp bands at 1882.0 and 1993.7 cm^{-1} that are probably due to MoH_6. These absorptions are much closer in frequency to those assigned to WH_6 than to (H_2)CrH_2(H_2). The MoH_6 molecule is clearly a classical hexahydride, like WH_6, and probably has the same trigonal prismatic structure, which is the calculated global minimum for MoH_6.[41]

The W/H_2/Ne sample reveals weak 2004.4 and 1927.5 cm^{-1} absorptions on deposition that alternatively increase on annealing and decrease on λ > 240 nm photolysis, which associates weaker 2021.2 and 1953.8 cm^{-1} W–H stretching modes (Fig. 8) and lower frequency 1080.3 and 840.7 cm^{-1} bands.[13] The distorted C_{3v} prism WH_6 structure contains three equivalent shorter W–H and three equivalent longer W–H bonds (Fig. 9). The two higher DFT calculated W–H stretching frequencies, a_1 and e modes, are predominantly due to the shorter trio of W–H bonds and the next two a_1 and e modes to the longer W–H bond trio based on computed displacement coordinates for each mode. The four W–H stretching modes calculated at 2059.3, 2039.9, 1963.7 and 1949.8 cm^{-1}, respectively, with the BPW91 functional (Table 6) as weak a_1, strong e, weak a_1 and strong e modes are 10–38 cm^{-1} (0.5–2%) higher but in excellent agreement with the observed 2021.2, 2004.4, 1953.8 and 1927.5 cm^{-1} bands. The a_1 and e deformation modes computed at 1151.1 and 894.0 cm^{-1} are observed at 1080.3 and 840.7 cm^{-1} in almost as good agreement. In conclusion, the overall excellent agreement between six calculated and observed frequencies for the distorted C_{3v} prism WH_6 structure confirms the identification, assignments, and structure of the novel WH_6 molecule formed and characterized in solid neon.[13–15] Although reaction 8 requires activation energy, which is calculated to be 28

Table 6 Neon matrix observed and DFT calculated frequencies (cm^{-1}) for WH_6 in the distorted trigonal prism structure

Observed[a]	Calculated[b]
2021.2 (3)	2059.3 (a_1, 45)
2004.4 (40)	2039.9 (e, 72 × 2)
1953.8 (12)	1963.7 (a_1, 92)
1927.5 (100)	1949.8 (e, 141 × 2)
1080.3 (30)	1155.1 (a_1, 101)
	946.1 (e, 14 × 2)
840.7 (14)	894.0 (e, 60 × 2)
	805.8 (a_2, 0)
	758.6 (a_1, 10)
	709.5 (e, 9 × 2)

[a] In solid neon, Ref. 13. Relative integrated band absorbances in parentheses. [b] Calculated at the BPW91/6-311G(d,p)/SDD level. Mode, intensity, km mol^{-1} in parentheses.

kcal mol^{-1},[79] this is provided by the laser-ablation process[17,24] or by photoexcitation, and reactions 9 and 10 appear to be spontaneous in the neon matrix.

$$W(^5D_o) + H_2\ (^1\Sigma_g^+) \rightarrow WH_2\ (^5B_2)\ \Delta E = -22\ \text{kcal mol}^{-1} \quad (8)$$

$$WH_2\ (^5B_2) + H_2\ (^1\Sigma_g^+) \rightarrow WH_4\ (^3A_1)\ \Delta E = -27\ \text{kcal mol}^{-1} \quad (9)$$

$$WH_4\ (^3A_1) + H_2\ (^1\Sigma_g^+) \rightarrow WH_6\ (^1A_1)\ \Delta E = -15\ \text{kcal mol}^{-1} \quad (10)$$

It is interesting to compare the reactivity of a bare W atom, the WH_2 molecule, $W(CO)_5$, and the Kubas subunit $W(CO)_3(PR_3)_2$ with the H_2 molecule. Although the bare W atom is unreactive,[79] excited W forms the dihydride WH_2, but WH_2 reacts straightaway with H_2 to give WH_4. However, the highly coordinated carbonyl complexes bind dihydrogen,[1-4,12] although the Kubas complex exists at equilibrium with the dihydride isomer at room temperature.[10] Clearly backbonding to CO decreases the capability of W to reduce the H_2 molecule to a classical hydride.

The only other known metal hexahydrides are MH_6^{x-} anions in solid ternary compounds with alkali or alkaline cations. These anions, however, have the regular octahedral structure,[80] and include $Re(III)H_6^{3-}$, $Fe(II)H_6^{4-}$, RuH_6^{4-}, OsH_6^{4-}, $Rh(III)H_6^{3-}$, IrH_6^{3-}, and $Pt(IV)H_6^{2-}$.[80–89] The infrared spectrum of Mg_2FeH_6 shows one strong absorption at 1720 cm^{-1}, which shifts to 1262 cm^{-1} in Mg_2FeD_6 (H/D ratio 1.363).[82] These bands are assigned to t_2 modes in the octahedral FeH_6^{4-} (FeD_6^{4-}) complexes, and they compare favorably to the antisymmetric FeH_2 stretching mode at 1726 cm^{-1} in the low-spin iron(II) complex *trans*-$[FeH_2(C_2H_4(PEt_2)_2)_2]$,[90] which is slightly higher than the linear FeH_2 molecule value (1661 cm^{-1}).[32] The structure and electron counting in homoleptic ternary transition metal hydride anions has been discussed.[80,91] These highly charged anions require adjacent cations for charge stabilization *via* interaction of the hydride anion ligands with the cations,[57] and they cannot be observed as isolated anions in solid matrices or in the gas phase.[92]

7 Conclusions

This review has focused on the variety of structures and states that can be formed from the elements for binary transition metal hydrides. The relative stabilities of matrix-isolated classical MH_2 dihydrides and $M(H_2)$ dihydrogen complexes in their own right and as subunits in higher hydrides has been explored. Celebrated examples are $Pd(H_2)$ and PtH_2, both of which form spontaneously in metal atom reactions with dihydrogen.[8,9,44,51] In addition palladium also yields the higher $Pd(H_2)_2$ and $Pd(H_2)_3$ complexes.[9] The stable gold trihydride is $(H_2)AuH$, and AuH_3 is a transition state that can be stabilized in the higher $(H_2)AuH_3$ complex.[72]

The matrix infrared experiment through the use of isotopic substitution on the vibrational frequencies (H_2, D_2, HD, $H_2 + D_2$) has proven to be an effective method for characterizing metal hydrides. Neon and argon matrix absorption spectra are slightly shifted from the gas phase frequencies[93] and hydrogen matrix absorptions typically fall between neon and argon matrix values.[94–96] The reaction dynamics are different in each matrix owing to different diffusion rates for H_2 in each condensing solid, and different product distributions are often observed (Table 5). Laser-ablation is an efficient technique for evaporating metal atoms,[24] particularly for the most refractory metals like tungsten, and this method finds many applications.

When dealing with new molecules it is very helpful to have the reinforcement of quantum chemical structure and vibrational frequency calculations. A large data base of vibrational frequencies computed with DFT using the hybrid B3LYP and pure BPW91 density functionals gives confidence to the vibrational assignments.[17,97,98] For a molecule as complicated as trigonal prismatic WH_6, the match between calculated and observed frequencies and infrared intensities is essential for confirmation of the matrix isolation preparation of this important hexahydride molecule.[13–15]

The use of pure normal hydrogen and deuterium as reagent and matrix is promising for the future discovery of new higher metal hydride molecules.[18,19,78,96,99] One advantage of molecular matrices is that the matrix itself can be monitored through weak induced infrared absorptions.[96,100,101] Finally, solid para-hydrogen has found application as a medium for spectroscopic investigations of atoms, molecules, and charged hydrogen clusters.[101–104]

Acknowledgement

The author gratefully acknowledges support from the (U.S.) National Science Foundation and the fruitful collaboration with X. Wang on the research described here.

References

1 G. J. Kubas, R. R. Ryan, B. I. Swanson, P. J. Vergamini and H. J. Wasserman, *J. Am. Chem. Soc.*, 1984, **106**, 451.
2 R. H. Crabtree, *Angew. Chem., Int. Ed. Engl.*, 1993, **32**, 789 and references therein.
3 G. J. Kubas, Metal Dihydrogen and σ-Bond Complexes, in *Modern Inorganic Chemistry*, Ed. J. P. Fackler Jr., Kluwer Academic/Plenum Publishers, New York, 2001 and references therein.
4 R. Poli and M. Pervzzini (Eds.), *Recent Advances in Hydride Chemistry*, Elsevier, Amsterdam, 2001 and references therein.
5 D. M. Heinekey and W. J. Oldham Jr., *Chem. Rev.*, 1993, **93**, 913.
6 B. R. Bender, G. J. Kubas, L. H. Jones, B. I. Swanson, J. Eckert, K. B. Capps and C. D. Hoff, *J. Am. Chem. Soc.*, 1977, **119**, 9179.
7 R. N. Perutz, *Pure. Appl. Chem.*, 1998, **70**, 2211.
8 G. A. Ozin and J. Garcia-Prieto, *J. Am. Chem. Soc.*, 1986, **108**, 3099 (Pd).
9 L. Andrews, X. Wang, M. E. Alikhani and L. Manceron, *J. Phys. Chem. A*, 2001, **105**, 3052 and references therein (Pd).
10 G. R. K. Khalsa, G. J. Kubas, C. J. Unkefer, L. S. Van Der Sluys and K. A. Kubat-Martin, *J. Am. Chem. Soc.*, 1990, **112**, 3855.
11 R. L. Sweany, *J. Am. Chem. Soc.*, 1985, **107**, 2374.
12 R. K. Upmacis, M. Poliakoff and J. J. Turner, *J. Am. Chem. Soc.*, 1986, **108**, 3645 and references therein.
13 X. Wang and L. Andrews, *J. Phys. Chem. A*, 2002, **106**, 6720 (W).
14 M. Shen, H. F. Schaefer III and H. Partridge, *J. Chem. Phys.*, 1993, **98**, 508.
15 M. Kaupp, *J. Am. Chem. Soc.*, 1996, **118**, 3018 and references therein.
16 T. R. Burkholder and L. Andrews, *J. Chem. Phys.*, 1991, **95**, 8697.
17 L. Andrews and A. Citra, *Chem. Rev.*, 2002, **102**, 885 and references therein.
18 R. J. Van Zee, S. Li and W. Weltner Jr., *J. Chem. Phys.*, 1995, **102**, 4367 and references therein (V, Nb).
19 X. Wang and L. Andrews, *J. Phys. Chem. A*, 2003, **107**, 570 and references therein (Cr).
20 R. J. Van Zee, T. C. DeVore, J. L. Wilkerson and W. Weltner Jr., *J. Chem. Phys.*, 1978, **69**, 1869(Mn).
21 R. L. Rubinowitz and E. R. Nixon, *J. Phys. Chem.*, 1986, **90**, 1940(Fe).

22 Z. L. Xiao, R. H. Hauge and J. L. Margrave, *J. Phys. Chem.*, 1991, **95**, 2696(Ti, V).
23 Z. L. Xiao, R. H. Hauge and J. L. Margrave, *J. Phys. Chem.*, 1992, **96**, 636 (Cr, Mo).
24 H. Kang and J. L. Beauchamp, *J. Phys. Chem.*, 1985, **89**, 3364.
25 M. J. Frisch, G. W. Trucks, H. B. Schlegel, G. E. Scuseria, M. A. Robb, J. R. Cheeseman, V. G. Zakrzewski, J. A. Montgomery, Jr., R. E. Stratmann, J. C. Burant, S. Dapprich, J. M. Millam, A. D. Daniels, K. N. Kudin, M. C. Strain, O. Farkas, J. Tomasi, V. Barone, M. Cossi, R. Cammi, B. Mennucci, C. Pomelli, C. Adamo, S. Clifford, J. Ochterski, G. A. Petersson, P. Y. Ayala, Q. Cui, K. Morokuma, D. K. Malick, A. D. Rabuck, K. Raghavachari, J. B. Foresman, J. Cioslowski, J. V. Ortiz, B. B. Stefanov, G. Liu, A. Liashenko, P. Piskorz, I. Komaromi, R. Gomperts, R. L. Martin, D. J. Fox, T. Keith, M. A. Al-Laham, C. Y. Peng, A. Nanayakkara, C. Gonzalez, M. Challacombe, P. M. W. Gill, B. G. Johnson, W. Chen, M. W. Wong, J. L. Andres, M. Head-Gordon, E. S. Replogle and J. A. Pople, *GAUSSIAN 98 (Revision A.6)*, Gaussian, Inc., Pittsburgh, PA, 1998 and references therein.
26 A. P. Scott and L. Radom, *J. Phys. Chem.*, 1996, **100**, 16502.
27 F. Maseras, A. Lledos, E. Clot and O. Eisenstein, *Chem. Rev.*, 2000, **100**, 601.
28 W. E. Billups, S.-C. Chang, R. H. Hauge and J. L. Margrave, *J. Am. Chem. Soc.*, 1995, **117**, 1387(Co).
29 T. M. Greene, W. Brown, L. Andrews, A. J. Downs, G. V. Chertihin, N. Runeberg and P. Pyykkö, *J. Phys. Chem.*, 1995, **99**, 7925 (Zn, Cd).
30 X. Wang, G. V. Chertihin and L. Andrews, *J. Phys. Chem. A*, 2002, **106**, 9213 (Sc, Y, La).
31 G. V. Chertihin and L. Andrews, *J. Am. Chem. Soc.*, 1994, **116**, 8322(Ti).
32 G. V. Chertihin and L. Andrews, *J. Phys. Chem.*, 1995, **99**, 1214 and references therein (Fe).
33 X. Wang and L. Andrews, *J. Phys. Chem. A*, 2003, **107**, 4081(Mn, Re).
34 S. Li, R. J. Van Zee, W. Weltner Jr., M. G. Cory and M. C. Zerner, *J. Chem. Phys.*, 1997, **106**, 2055(Ni).
35 X. Wang, L. Andrews, L. Manceron and C. Marsden, *J. Phys. Chem. A*, 2003, **107**, 8492 (Cu, Ag, Au).
36 H. Körsgen, W. Urban and J. M. Brown, *J. Chem. Phys.*, 1999, **110**, 3861.
37 J. R. Barron and R. Liu, *J. Chem. Phys.*, 1998, **108**, 1.
38 G. A. Ozin and C. Gracie, *J. Phys. Chem*, 1984, **88**, 643.
39 J. Garcia-Prieto, M. E. Ruiz and O. Novaro, *J. Am. Chem. Soc.*, 1985, **107**, 5635.
40 G. V. Chertihin and L. Andrews, *J. Phys. Chem.*, 1995, **99**, 15004 (Zr,Hf) and references therein.
41 X. Wang and L. Andrews, to be published (Mo).
42 X. Wang and L. Andrews, to be published (Fe, Ru).
43 X. Wang and L. Andrews, *J. Phys. Chem. A*, 2002, **106**, 3706 (Rh).
44 L. Andrews, X. Wang and L. Manceron, *J. Chem. Phys.*, 2001, **114**, 1559 (Pt).
45 N. Legay-Sommaire and F. Legay, *Chem. Phys. Lett.*, 1993, **207**, 123(Hg).
46 P. Pyykkö, *Chem. Rev.*, 1988, **88**, 563 and references therein.
47 P. Schwerdtfeger, W. H. E. Schwarz, G. A. Bowmaker and P. D. W. Boyd, *J. Chem. Phys.*, 1989, **91**, 1762.
48 P. Schwerdtfeger, P. D. W. Boyd, S. Brienne and A. K. Burrell, *Inorg. Chem.*, 1992, **31**, 3411 and references therein.
49 K. Balsubramanian, *J. Chem. Phys.*, 1987, **87**, 2800.
50 K. Balusubramanian and D. Dai, *J. Chem. Phys.*, 1990, **93**, 7243.
51 M. E. Alikhani and C. Minst, *J. Phys. Chem. A*, 2003, **107**, 5352.
52 K. P. Huber and G. Herzberg, *Molecular Spectra and Molecular Structure. IV. Constants of Diatomic Molecules*; Van Nostrand Reinhold, New York, 1979.
53 L. Andrews and X. Wang, *J. Am. Chem. Soc.*, 2003, **125**, 11751.
54 K. Balusubramanian and M. J. Liao, *J. Phys. Chem.*, 1988, **92**, 361.
55 A. E. S. Miller, C. S. Feigerle and W. C. Lineberger, *J. Chem. Phys.*, 1986, **84**, 4127.
56 M. Kritikos, D. Noréus, A. F. Andersen and P. Fischer, *Solid State Chem.*, 1991, **92**, 514.
57 M. Olofsson-Mårtensson, U. Häussermann, J. Tomkinson and D. Noréus, *J. Am. Chem. Soc.*, 2000, **122**, 6960.
58 W. Bronger and G. Auffermann, *J. Alloys Comp.*, 1995, **228**, 119.
59 N. B. Balbanov and J. E. Boggs, *J. Phys. Chem. A*, 2000, **104**, 1597.
60 J. A. Osborn, F. H. Jardine, J. F. Young and G. Wilkinson, *J. Chem. Soc. A*, 1966, 1711.
61 K. C. Dewhirst, W. Keim and C. A. Reilly, *Inorg. Chem.*, 1968, **7**, 546.
62 T. Ito, S. Kitazume, A. Yamamoto and S. Ikeda, *J. Am. Chem. Soc.*, 1970, **92**, 3011.
63 E. Wiberg and H. Neumaier, *Inorg. Nucl. Chem. Lett*, 1965, **1**, 35.
64 H. Lehner, D. Matt, P. S. Pregosin, L. M. Venanzi and A. J. Albinati, *J. Am. Chem. Soc.*, 1982, **104**, 6825.
65 D. B. Alexander, B. J. Johnson, S. M. Johnson, A. L. Casalnuovo and L. H. Pignolet, *J. Am. Chem. Soc.*, 1986, **108**, 4409.
66 A. Albinati, H. Lehner, L. M. Venanzi and M. Wolfer, *Inorg. Chem.*, 1987, **26**, 3933.
67 A. Albinati, C. Anklin, P. Janser, H. Lehner, D. Matt, P. S. Pregosin and L. M. Venanzi, *Inorg. Chem.*, 1989, **28**, 1105.
68 C. A. Bayse and M. B. Hall, *J. Am. Chem. Soc*, 1999, **121**, 1348.
69 C. A. Bayse, *J. Phys. Chem. A*, 2001, **105**, 5902.
70 N. B. Balabanov and J. E. Boggs, *J. Phys. Chem. A*, 2001, **105**, 5906.
71 P. Pyykkö, *J. Am. Chem. Soc.*, 1995, **117**, 2067.
72 X. Wang and L. Andrews, *J. Phys. Chem. A*, 2002, **106**, 3744 (Au).
73 X. Wang and L. Andrews, *J. Am. Chem. Soc.*, 2002, **124**, 7610 (YH_4^-).
74 D. E. Milligan and M. E. Jacox, *J. Mol. Spectrosc.*, 1973, **46** , 460.
75 C. A. Wight, B. S. Ault and L. Andrews, *J. Chem. Phys.*, 1976, **65**, 1244.
76 B. Ma, C. L. Collins and H. F. Schaefer III, *J. Am. Chem. Soc.*, 1996, **118**, 870.
77 T. Y. Cheng and R. M. Bullock, *J. Am. Chem. Soc.*, 1999, **121**, 3150.
78 L. Manceron, to be published (Pd).
79 Z. Ma and K. Balusubramanian, *Chem. Phys. Lett.*, 1991, **181**, 467.
80 R. B. King, *Coord. Chem. Rev.*, 2000, **200–202**, 813 and references therein.
81 W. Bronger, G. A. Auffermann and H. Schilder, *Z. Anorg. Allg. Chem.*, 1998, **624**, 497.
82 J. J. Didisheim, P. Zolliker, K. Yvon, P. Fischer, J. Schefer, M. Gubelmann and A. F. Williams, *Inorg. Chem.*, 1984, **23**, 1953.
83 B. Huang, F. Bonhomme, P. Selvam, K. Yvon and P. Fischer, *J. Less Common Metals*, 1991, **171**, 301.
84 B. Huang, K. Yvon and P. Fischer, *J. Alloys Compd.*, 1995, **227**, 121.
85 B. Huang, F. Gingl, F. Fauth, A. Hewat and K. Yvon, *J. Alloys Compd.*, 1997, **248**, 13.
86 W. Bonger, M. Gehlen and G. Auffermann, *Z. Anorg. Allg. Chem.*, 1994, **620**, 1983.
87 J. E. Ellis, P. T. Barger and M. L. Winzenburg, *J. Chem. Soc., Chem. Commun.*, 1977, 686.
88 W. Bonger and G. Auffermann, *Angew. Chem., Int. Ed. Engl.*, 1994, **33**, 1112.
89 W. Bonger and G. Auffermann, *Z. Anorg. Allg. Chem.*, 1995, **621**, 1318.
90 J. Chatt and R. G. Hayter, *J. Chem. Soc.*, 1961, 5507.
91 T. K. Firman and C. R. Landis, *J. Am. Chem. Soc.*, 1998, **120**, 12650.
92 L. S. Wang and X. B. Wang, *J. Phys. Chem. A*, 2000, **104**, 1978 and references therein.
93 M. E. Jacox, *Chem. Phys.*, 1994, **189**, 149.
94 L. Li, J. T. Graham and W. Weltner Jr., *J. Phys. Chem. A*, 2001, **105**, 11018.
95 X. Wang, L. Andrews, G. V. Chertihin and P. F. Souter, *J. Phys. Chem. A*, 2002, **106**, 6302 (Sn, Pb).
96 X. Wang and L. Andrews, *J. Am. Chem. Soc.*, 2003, **125**, 6581(PbH_4).
97 M. F. Zhou, L. Andrews and C. W. Bauschlicher Jr., *Chem. Rev.*, 2001, **101**, 1931.
98 F. S. Legge, G. L. Nyberg and J. B. Peel, *J. Phys. Chem. A*, 2001, **105**, 7905.
99 L. Andrews and X. Wang, *Science*, 2003, **299**, 2049 (Al_2H_6).
100 A. Crane and H. P. Gush, *Can. J. Phys.*, 1966, **44**, 373 and references therein.
101 S. Tam, M. Macler and M. E. Fajardo, *J. Chem. Phys.*, 2000, **113**, 9067.
102 T. Momose and T. Shida, *Bull. Chem. Soc. Japan*, 1998, **71**, 1.
103 N. Sogoshi, Y. Kato, T. Wakabayashi, T. Momose, S. Tam, M. E. DeRose and M. E. Fajardo, *J. Phys. Chem. A*, 2000, **16**, 3733.
104 M.-C. Chan, M. Okumara and T. Oka, *J. Phys. Chem. A*, 2000, **104**, 3775.